

# A Series of NiM (M = Ru, Rh, and Pd) Bimetallic Catalysts for Effective Lignin Hydrogenolysis in Water

Jianguang Zhang,<sup>†</sup> Jason Teo,<sup>†</sup> Xi Chen,<sup>†</sup> Hiroyuki Asakura,<sup>‡</sup> Tsunehiro Tanaka,<sup>§,¶</sup> Kentaro Teramura,<sup>§,¶,||</sup> and Ning Yan<sup>\*,†</sup>

<sup>†</sup>Department of Chemical and Biomolecular Engineering, National University of Singapore, 4 Engineering Drive 4, 117585, Singapore

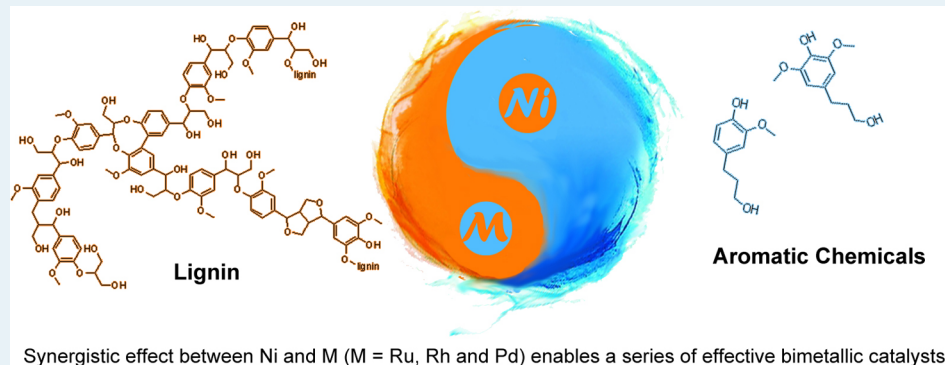
<sup>‡</sup>Synchrotron Radiation Research Center, Nagoya University, Chikusa-ku, Nagoya 464-8603, Japan

<sup>§</sup>Department of Molecular Engineering, Graduate School of Engineering, Kyoto University, Kyoto 615-8510, Japan

<sup>¶</sup>Elements Strategy Initiative for Catalysts and Batteries (ESICB), Kyoto University, Kyoto, 615-8520, Japan

<sup>||</sup>Precursory Research for Embryonic Science and Technology (PRESTO), Japan Science and Technology Agency (JST), 4-1-8 Honcho, Kawaguchi, Saitama 332-0012, Japan

## Supporting Information



**ABSTRACT:** In this paper, NiRu, NiRh, and NiPd catalysts were synthesized and evaluated in the hydrogenolysis of lignin C–O bonds, which is proved to be superior over single-component catalysts. The optimized NiRu catalyst contains 85% Ni and 15% Ru, composed of Ni surface-enriched, Ru–Ni atomically mixed, ultrasmall nanoparticles. The Ni<sub>85</sub>Ru<sub>15</sub> catalyst showed high activity under low temperature (100 °C), low H<sub>2</sub> pressure (1 bar) in  $\beta$ -O-4 type C–O bond hydrogenolysis. It also exhibited significantly higher activity over Ni and Ru catalysts in the direct conversion of lignin into monomeric aromatic chemicals. Mechanistic investigation indicates that the synergistic effect of NiRu can be attributed to three factors: (1) increased fraction of surface atoms (compared with Ni), (2) enhanced H<sub>2</sub> and substrate activation (compared with Ni), and (3) inhibited benzene ring hydrogenation (compared with Ru). Similarly, NiRh and NiPd catalysts were more active and selective than their single-component counterparts in the hydrogenolysis of lignin model compounds and real lignin.

**KEYWORDS:** lignin, hydrogenolysis, NiRu, aromatic chemicals, bimetallic

## INTRODUCTION

Lignin, composing 15–30 wt % of lignocellulosic biomass and carrying 40% of its energy, is an attractive fraction in the woody biomass in future biorefinery.<sup>1</sup> The major repeating units of lignin are orthomethoxy-substituted C<sub>9</sub> phenolic moieties, which are cross-linked by C–O bonds, including  $\beta$ -O-4,  $\alpha$ -O-4, and 4-O-5 linkages (see Figure 1), and additionally by C–C bonds.<sup>2</sup> Because of this unique structure, lignin represents an ideal renewable source for the production of value-added aromatic chemicals.<sup>3</sup> Hydrogenolysis of C–O linkages in lignin, in which H<sub>2</sub> is used to cleave the C–O bond over a metal catalyst, is regarded as an effective way to transform lignin into depolymerized aromatic platform compounds.<sup>4</sup> Unfortunately, several technological and scientific breakthroughs, such as the

development of highly effective catalyst, are required to make lignin hydrogenolysis industrially viable.<sup>5</sup>

Despite the long-standing practice of metal-catalyzed lignin hydrogenolysis,<sup>6</sup> the catalyst-designing strategy remains limited. A wide variety of catalysts, based either on noble<sup>7</sup> or non-noble metals,<sup>8</sup> have been attempted. Noble metal catalysts typically include Ru, Rh, Pd, or Pt loaded on various supports. For example, Ru on activated carbon was used to convert wood lignin and cornstalk into phenolic compounds and alkanes in a water–dioxane<sup>9</sup> or water–ethanol mixture.<sup>10</sup> A combination of Pd/C and HZSM-5 catalysts were used to convert a  $\beta$ -O-4 model

Received: December 16, 2013

Revised: April 7, 2014

Published: April 8, 2014

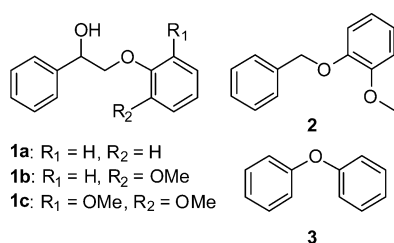


**Figure 1.**  $\beta$ -O-4 (**1a–c**),  $\alpha$ -O-4 (**2**), and 4-O-5 (**3**) lignin model compounds used in this study.

compound to  $C_6$ -cyclohexane and  $C_8$ -ethylcyclohexane at 200 °C under 5 MPa  $H_2$ .<sup>11</sup> A homogeneous ruthenium–xantphos catalyst was employed for hydrogenolysis of lignin model dimers at 135 °C for 20 h in toluene with a high yield of hydrogenolysis products.<sup>7d</sup> Although noble metal catalysts show promising activity and efficiency, these low-abundance, precious elements are not suitable as predominant catalyst components in large-scale processes, such as lignin transformation. In addition, noble metal catalysts generally exhibit undesired activity in benzene ring hydrogenation,<sup>12</sup> leading to extra consumption of hydrogen and decreased yield of targeted aromatic chemicals.

Non-noble metal catalysts are mainly based on Cu,<sup>13</sup> Fe,<sup>14</sup> and, in particular, Ni.<sup>15</sup> Ni is widely used as a hydrogenation catalyst because of its low cost and moderate activity. However, the application of Ni for lignin hydrogenolysis has not received considerable attention until recently. In 2011, a soluble nickel carbene complex, which attains high selectivity of aromatic products in organic solvents, was adopted as the catalyst for the hydrogenolysis of 4-O-5 type of lignin model compounds.<sup>15a</sup> Heterogeneous Ni catalysts, such as Ni/ $K_2CO_3$ / $ZrO_2$ , have been used to cleave the C–O bonds in lignin, but they are effective only under severe conditions (240–400 °C, 25–32 MPa  $H_2$ ).<sup>15b–d</sup> Following that, hydrogenolysis of lignin model compounds and real lignin over Ni/HZSM-5 catalyst under moderate conditions (250 °C, 5 MPa  $H_2$ ) was demonstrated.<sup>11</sup> Ni/ $SiO_2$ <sup>15e</sup> and Ni/C<sup>15f</sup> catalysts were reported to promote lignin hydrogenolysis under milder conditions in environmentally benign solvents (120–200 °C, 6–50 bar  $H_2$  in water or ethylene glycol). Recently, lignin depolymerization by Ni on layered double hydroxide catalysts was developed.<sup>15g</sup> Nevertheless, further improvements of Ni-based catalysts is desirable because of the limited activity at low temperatures (generally inactive at temperatures below 120 °C) and poor dispersion of the Ni catalyst.

Very recently, we reported a NiAu catalyst that is more active than pure Ni catalyst under the same preparation and reaction conditions in lignin hydrogenolysis (pure Au is inert for the reaction).<sup>16</sup> Encouraged by this, the synergistic effects in three other NiM (M = Ru, Rh, and Pd) catalysts were evaluated in detail in this study. Each component in the bimetallic catalyst is active in lignin hydrogenolysis, but their combination leads to improved catalytic performance, overcoming the limitations of both pure Ni and noble metal catalysts. It is well documented that the combination of two metals could result in drastically enhanced catalytic performance, and the employment of bimetallic catalysts dates back to the 1970s.<sup>17</sup> However, as far as we are aware, this approach has not been utilized to develop catalysts for lignin valorization.

## EXPERIMENTAL SECTION

**Materials.** Sodium borohydride ( $NaBH_4$ , 95% purity) was purchased from TCI. Polyvinylpyrrolidone (PVP, MW = 40 000) was from Alfa Aesar. Ruthenium(III) chloride hydrate ( $RuCl_3 \cdot xH_2O$ , Ru content 37 wt %), rhodium(III) chloride hydrate ( $RhCl_3 \cdot xH_2O$ , Rh content 38.95 wt %), palladium(II) chloride, nickel(II) chloride hydrate ( $NiCl_2 \cdot 6H_2O$ , 98% purity), and potassium carbonate were provided by Sinopharm Chemical Reagent. Phenol, 2-bromoacetophenone, guaiacol, 2,6-dimethoxyphenol, and benzyl bromide were from Sigma-Aldrich. Acetone, ethanol, ethyl acetate, hexane, diethyl ether, and diphenyl ether were purchased from Fisher.  $H_2$  (99.995%) was ordered from SOXAL, Singapore. All chemicals were used as received.

**Instrumentations.** Hydrogenolysis products were analyzed by gas chromatography (GC) and gas chromatography/mass spectroscopy (GC/MS) on an Agilent 7890A gas chromatograph with a flame ionization detector (FID) and an Agilent 7890A-5975 GC/MS instrument, both equipped with HP-5 capillary columns (30 m  $\times$  250  $\mu$ m). Gel permeation chromatography (GPC) analysis was carried out with a system equipped with a Waters 2410 refractive index detector, a Waters 515 HPLC pump and two Waters styragel columns (HT 3 and HT 4) using 0.1 M LiCl/DMF as eluent at a flow rate of 1 mL/min at 25 °C. The raw data were processed using narrow polystyrenes as calibrations on the software Breeze. Transmission electron microscopy (TEM) images were taken using a JEOL JEM-2010 microscope operating at 200 kV. X-ray photoelectron spectroscopy (XPS) measurements were performed on a VG Escalab MKII spectrometer, using a mono Al  $K\alpha$  X-ray source ( $h\nu = 1486.71$  eV, 5 mA, 15 kV) and calibrated by setting the C 1s peak to 285.0 eV. X-ray powder diffraction (XRD) was performed on a Bruker D8 Advanced Diffractometer with Cu  $K\alpha$  radiation at 40 kV. UV–vis spectra were recorded on a Shimadzu 3600 UV–vis spectrophotometer equipped with a CPS-240A controller. Ni K-edge X-ray absorption spectra (XAS) of the NiRu and NiRh catalysts and reference samples (Ni foil, and NiO) were recorded at the BL01B1 beamline at the SPring-8 (Japan Synchrotron Radiation Research Institute, Hyogo, Japan) in the transmission mode at ambient temperature. A Si (111) double crystal monochromator was used to obtain a monochromatic X-ray beam. The monochromator was calibrated at the shoulder peak of the absorption edge of an X-ray absorption near edge structure (XANES) spectrum of Cu foil. Ru and Rh K-edge XAS of the catalysts and reference samples (Ru powder, Rh foil, and  $RuO_2$ ) were also recorded in the same manner except for the use of a Si (311) double crystal monochromator. The monochromator was calibrated at the inflection point of the XANES spectrum of the metal powder/foil. In both cases, higher harmonics were removed by changing glancing angles of collimation and focusing mirrors. Data reduction was carried out with Athena and Artemis included in the Iffeffit and Demeter package.<sup>18</sup> For curve-fitting analysis on extended X-ray absorption fine structure (EXAFS) spectra, each theoretical scattering path was generated with FEFF 6.0L,<sup>19</sup> and amplitude reduction factors were estimated by the curve-fitting on the reference metal samples. The  $k^2$ -weighted EXAFS oscillation in the range of 3.0–13  $\text{\AA}^{-1}$  was Fourier transformed, and curve-fitting analyses were performed in the range 1.4–2.8  $\text{\AA}$  in R space.

**Preparation of Catalysts.** (a)  $Ni_xRu_{100-x}$  Catalysts. A series of  $Ni_xRu_{100-x}$  catalysts ( $x = 0, 75, 80, 85, 90, 95, 100$ , where  $x$  represents the molar percentage of Ni) were prepared using a wet

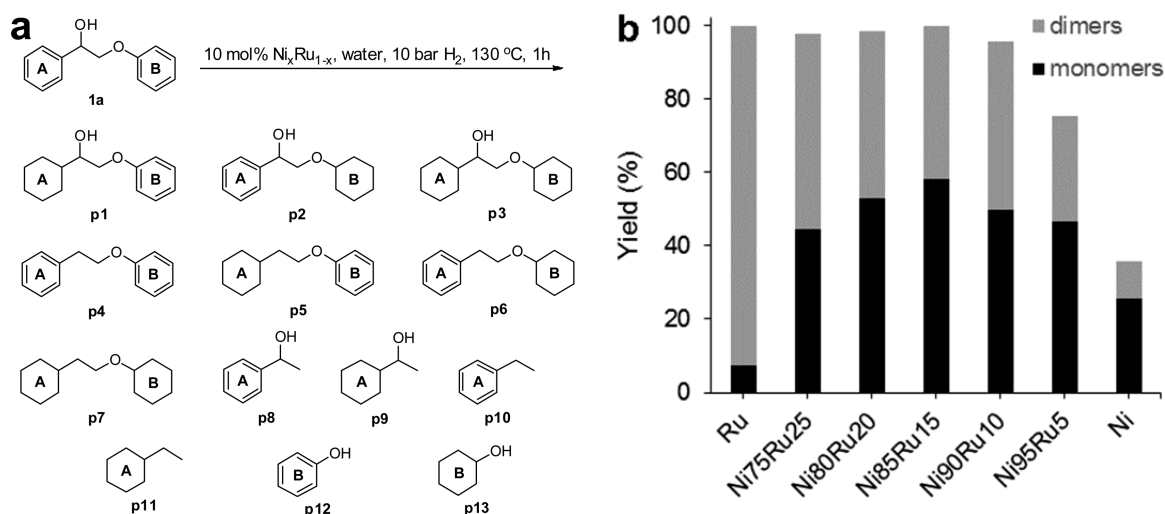


**Figure 2.** (a) Thirteen products identified after **1a** hydrogenolysis; (b) yields of monomers and dimers over Ni, Ru, and NiRu with varying Ni/Ru ratio. Reaction conditions: 0.22 mmol **1a**, 3 mL of freshly prepared aqueous solution containing 0.022 mmol of metal and 0.44 mmol of PVP, 10 bar H<sub>2</sub>, 130 °C, 1 h.

chemical method employing PVP as stabilizer and NaBH<sub>4</sub> as reductant.<sup>20</sup> A typical preparation procedure for Ni<sub>85</sub>Ru<sub>15</sub> is described here. To an aqueous solution (2 mL) of NiCl<sub>2</sub>·6H<sub>2</sub>O (4.4 mg, 0.0187 mmol), RuCl<sub>3</sub>·xH<sub>2</sub>O (0.9 mg, 0.0033 mmol), and PVP (48.8 mg, 0.44 mmol based on monomer), a freshly prepared aqueous solution of NaBH<sub>4</sub> (4 mg, 0.11 mmol, in 1 mL H<sub>2</sub>O) was added in one portion under vigorous stirring. A black colloid was obtained immediately, which was transferred into a reactor after ~30 s and used for the catalytic reaction.

(b). *Ni<sub>x</sub>Rh<sub>100-x</sub> Catalysts.* The Ni<sub>x</sub>Rh<sub>100-x</sub> ( $x = 0, 60, 65, 70, 75, 80, 85, 90, 95, 100$ , where  $x$  represents the molar percentage of Ni) catalysts were prepared using a procedure identical to that described for Ni<sub>x</sub>Ru<sub>100-x</sub> catalysts except that RhCl<sub>3</sub>·xH<sub>2</sub>O was used as the Rh precursor.

(c). *Ni<sub>85</sub>Pd<sub>15</sub> Catalyst.* PdCl<sub>2</sub> (0.6 mg, 0.0033 mmol) was dissolved in an aqueous solution (2 mL) containing NaCl (0.0198 mmol) to form Na<sub>2</sub>PdCl<sub>4</sub>. To this solution, NiCl<sub>2</sub>·6H<sub>2</sub>O (4.4 mg, 0.0187 mmol), and PVP (48.8 mg, 0.44 mmol based on monomer) were added, and the suspension was stirred for 30 s for dissolution. The following procedure was identical to that of Ni<sub>x</sub>Ru<sub>100-x</sub> catalysts described above.

**Hydrogenolysis Reaction with Model Compounds.** Model compounds **1a**, **1b**, **1c**, and **2** were synthesized following a modified literature procedure.<sup>21</sup> The full procedure and NMR data can be found in the Supporting Information (SI).

In a typical experiment, the substrate (0.22 mmol), fresh catalyst (0.022 mmol metal and 0.44 mmol PVP in 3 mL H<sub>2</sub>O), and a magnetic stirrer were placed into a high-pressure reactor (20 mL). After flushing with H<sub>2</sub> three times, the reactor was charged with 10 bar of H<sub>2</sub> and placed into a preheated oil bath with a stirring speed of 1000 rpm. After the reaction, the reactor was quenched to ambient temperature using cooling water, and the organic products were extracted using ethyl acetate (6 mL) and analyzed by GC-FID and GC/MS. The response factor for each component was calculated using the effective carbon number (ECN).<sup>22</sup> The yield is defined as the molar amount of C<sub>6</sub> rings in the individual product divided by the total moles of C<sub>6</sub> rings in the starting materials. Because the carbon balance was high (90–95%), the GC area normalization method was used to determine the yield, which is given by dividing the molar amount

of C<sub>6</sub> rings in this product by the total moles of C<sub>6</sub> rings detected on GC-FID:

$$\text{yield}_x(\%) = \frac{n \times \text{area}_x / \text{ECN}_x}{\sum(\text{area}_i / \text{ECN}_i) + 2 \times \sum(\text{area}_j / \text{ECN}_j) + 2 \times \text{area}_{\text{sub}} / \text{ECN}_{\text{sub}}}$$

where  $n$  is the number of C<sub>6</sub> ring(s) in each product (e.g.,  $n = 1$  for monomers, and  $n = 2$  for dimers),  $i$  is subscript for monomers,  $j$  is subscript for dimers, and sub is the subscript for substrates.

The specific reaction conditions can be found in the figure captions and table footnotes.

**Depolymerization of Organosolv Lignin.** Organosolv lignin was extracted from birch wood sawdust following a literature method.<sup>23</sup> The reaction conditions were similar to model compound hydrogenolysis reactions, except that they employed organosolv lignin (50 mg) as the substrate. After reaction, the reactor was quenched to ambient temperature using cooling water. The reaction suspension was extracted with ethyl acetate (6 mL × 3). The organic phases were combined and concentrated over a rotary evaporator. The aqueous phase suspension was centrifuged, and the solid residue was washed with water (3 mL × 3) to recover unconverted lignin. Methanol (0.5 mL) was added to dissolve the residues, following which *n*-dodecane (10 μL) was added as an internal standard. The solution was finally analyzed by GC-FID and GC/MS. The response factor for each product was calculated by the ECN, and its mass yield was determined by dividing its mass (calculated by referencing the internal standard) by 50 mg (the mass of starting organosolv lignin):

$$\text{yield}_x(\text{wt}\%) = \frac{(\text{mass}_{n\text{-dodecane}}(\text{mg}) / 170) \times \frac{\text{area}_x / \text{ECN}_x}{\text{area}_{n\text{-dodecane}} / 12} \times \text{MW}_x}{50(\text{mg})} \times 100\%$$

**In Situ Uv–Vis.** For in situ observation of a metal reduction process, an aqueous solution (2.0 mL) containing PVP (16.5 mM) and metal precursor (0.825 mM, either NiCl<sub>2</sub>, RuCl<sub>3</sub> or a 85:15 combination of the two) was transferred into a standard quartz cell at 16 °C. After addition of a freshly prepared aqueous

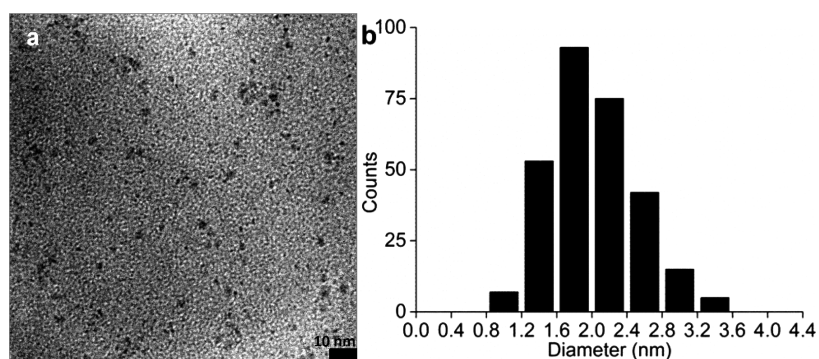


**Figure 3.** (a) TEM image and (b) size distribution of  $\text{Ni}_{85}\text{Ru}_{15}$  catalyst.

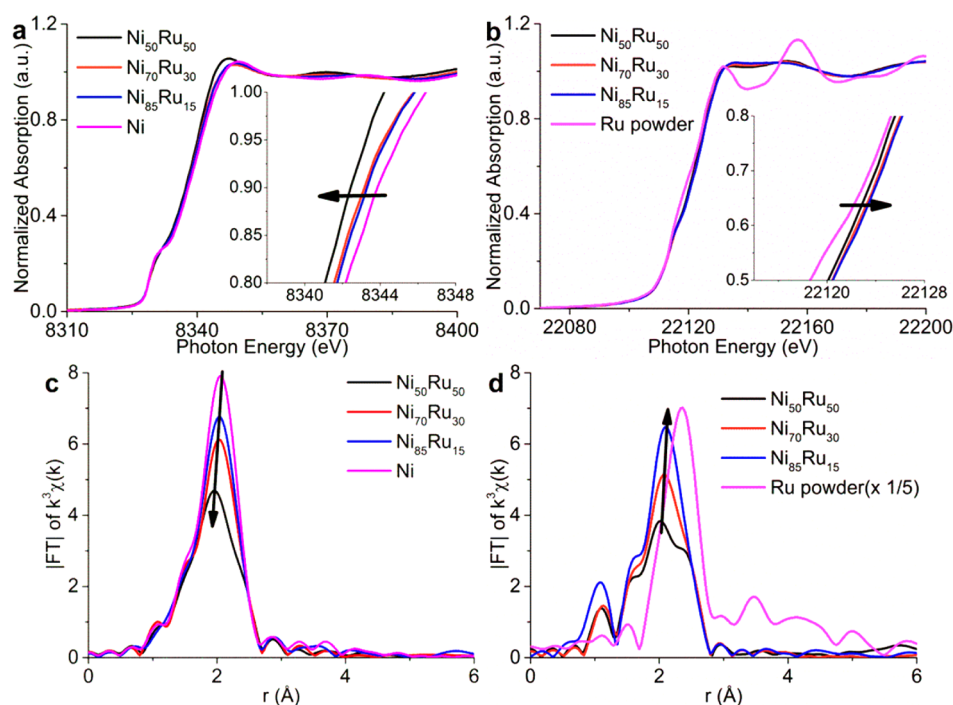


**Figure 4.** (a) Ni and (b) Ru K-edge XANES spectra of Ni,  $\text{Ni}_{85}\text{Ru}_{15}$ ,  $\text{Ni}_{70}\text{Ru}_{30}$ ,  $\text{Ni}_{50}\text{Ru}_{50}$  catalysts and a Ru powder reference. Fourier transformed (c) Ni and (d) Ru K-edge EXAFS spectra of Ni,  $\text{Ni}_{85}\text{Ru}_{15}$ ,  $\text{Ni}_{70}\text{Ru}_{30}$ , and  $\text{Ni}_{50}\text{Ru}_{50}$  catalysts and a Ru powder reference.

solution of  $\text{NaBH}_4$  (8.25 mM, 1.0 mL) maintained at the same temperature, the mixture was monitored continuously by UV–vis at 250–600 nm range with a time interval of 2 min.

## RESULTS AND DISCUSSION

**NiRu Catalysts.** We prepared Ni, Ru, and  $\text{Ni}_x\text{Ru}_{100-x}$  catalysts in aqueous phase by reducing  $\text{NiCl}_2 \cdot 6\text{H}_2\text{O}$ ,  $\text{RuCl}_3 \cdot x\text{H}_2\text{O}$  or their combinations with  $\text{NaBH}_4$  in the presence of PVP as a stabilizing agent. The prepared catalysts were immediately tested in the hydrogenolysis of 2-phenoxy-1-phenethanol (**1a**), a typical model compound bearing lignin  $\beta$ -O-4 type linkage, at 130 °C with 10 bar  $\text{H}_2$  for 1 h. Thirteen products were observed after the reaction (**p1–p13**; see Figure 2a). Compounds **p8–p13**, which bear only one  $\text{C}_6$  ring structure derived from either ring A or ring B through C–O bond hydrogenolysis, are denoted as monomers. Compounds **p1–p7** are dimers generated by hydrogenation of the substrate without the cleavage of the C–O bond. Thus, total monomer yield can act as an indicator of hydrogenolysis activity of catalysts, whereas the total yield of dimers can represent hydrogenation activity partially.

Product yields over different catalysts are compiled in Figure 2b (for the detailed yield of each product, see Table S1 in the SI). Ni monometallic catalyst achieved 36% conversion and 70% selectivity toward monomers. In contrast, the Ru catalyst showed higher activity ( $\sim 100\%$ ), but the monomer yield was only 8%. By incorporating Ru into Ni, the NiRu catalysts inherited the advantages of both components, in which Ru increased the total activity of Ni, and Ni tuned the selectivity of Ru to favor the C–O bond cleavage. This synergistic effect, with the increasing Ru content, reached a peak by using  $\text{Ni}_{85}\text{Ru}_{15}$ , over which 100% conversion with 58% monomer yield was achieved. The activity of higher-Ru-content catalysts was maintained while the selectivity of monomers dropped gradually. Thus,  $\text{Ni}_{85}\text{Ru}_{15}$  was chosen to be further investigated.

Several characterization techniques were applied to probe the structure of the  $\text{Ni}_{85}\text{Ru}_{15}$  catalyst. TEM analysis indicates that the  $\text{Ni}_{85}\text{Ru}_{15}$  catalyst is spherical with a diameter of  $2.0 \pm 0.5$  nm (see Figure 3a,b), similar to pure Ru catalyst (2 nm) but much smaller than the Ni catalyst ( $11.5 \pm 3.5$  nm) (see SI Figure S1 for TEMs). SI Figure S2 shows the XRD pattern of  $\text{Ni}_{85}\text{Ru}_{15}$  catalyst. Several sets of peaks attributed to the byproducts ( $\text{NaCl}$  and  $\text{NaBO}_2$ )

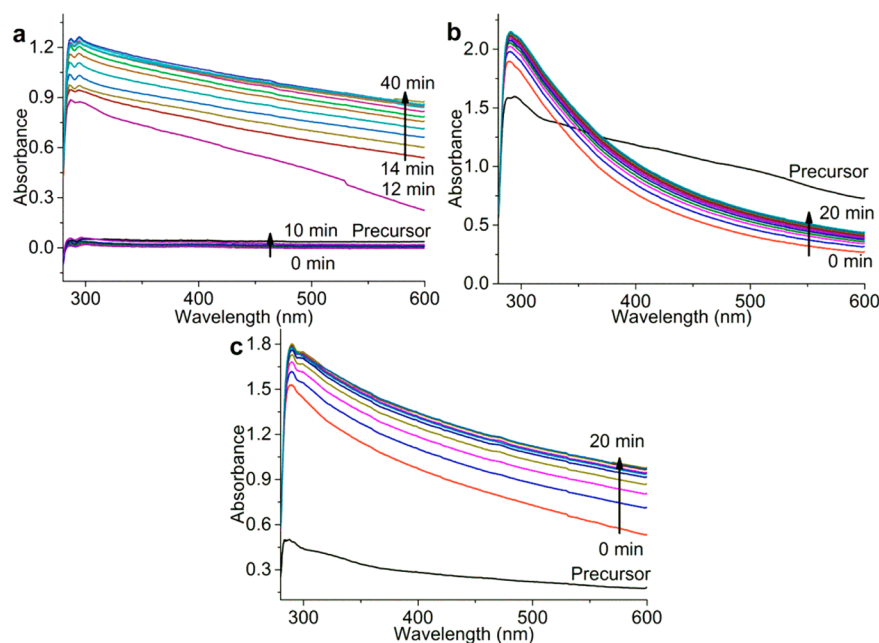


**Figure 5.** In situ UV–vis spectra recorded during the preparation of (a) Ni, (b) Ru, and (c) Ni<sub>85</sub>Ru<sub>15</sub> catalysts. Spectra were recorded every 2 min. Reaction conditions: 2 mL of water solution containing 0.00165 mmol of metal precursors and 0.033 mmol of PVP and 1 mL of NaBH<sub>4</sub> (0.00825 mmol) solution were added; pure water as reference.

generated during the reduction were observed. The two broad peaks at  $2\theta = 10^\circ$  and  $20^\circ$  were attributed to PVP.<sup>24</sup> Except for these peaks, there are no diffraction peaks for metals in the XRD pattern, corresponding to the small size of Ni<sub>85</sub>Ru<sub>15</sub> observed in TEM image.

XPS was employed to characterize valence state and surface composition of catalysts. As shown in SI Figure S3, the spectra for Ni and Ni<sub>85</sub>Ru<sub>15</sub> in Ni 2p region are quite similar, revealing oxidation of Ni has occurred during the sample preparation. Because of the relatively small Ru composition and high PVP content, the Ru 3d signal is obscured by large C 1s peaks in both Ru and Ni<sub>85</sub>Ru<sub>15</sub>. Nevertheless, the appearance of the Ru 3p peak indicates the existence of near-surface Ru in the Ni<sub>85</sub>Ru<sub>15</sub> catalyst. Using the Ru 3p<sub>3/2</sub> and Ni 2p<sub>3/2</sub> peak areas, the surface ratio of Ni/Ru can be determined as 9.0:1, which is higher than the precursors' ratio, 5.7:1, indicating that Ni is probably surface-enriched.

X-ray absorption spectroscopy was conducted to inspect the electronic states and morphology of the catalysts at atomic scale.<sup>25</sup> For a systematic comparison, we prepared Ni, Ni<sub>85</sub>Ru<sub>15</sub>, Ni<sub>70</sub>Ru<sub>30</sub>, and Ni<sub>50</sub>Ru<sub>50</sub> in appropriate concentration for XAFS measurements. The catalysts were prepared on site and measured immediately after synthesis to prevent Ni oxidation. As shown in Figure 4a,b, both the Ni K-edge XANES spectra of NiRu and Ni, and the Ru K-edge XANES spectra of NiRu and Ru powder are similar, indicating both Ru and Ni are in the metallic state. On the other hand, small but systematic changes in their absorption edges are observed; that is, the edge shifts toward lower energy at the Ni K-edge as the Ru content increases and to the higher energy at the Ru K-edge as the Ni content increases. This suggests the charge transfer from Ru to Ni in the NiRu bimetallic catalyst.

Figure 4c,d shows the Fourier transformed EXAFS (FT-EXAFS) of the NiRu catalyst at the Ni and Ru K-edge. The first peaks at around 1.9 Å at the Ni K-edge and at around 2.0 Å at the Ru K-edge systematically decreased as the Ru content increased. As clearly shown in SI Figure S1, Ru nanoparticles tend to be

smaller than Ni NPs under the present preparation conditions. Thus, the change in FT-EXAFS spectra could be interpreted as the generation of smaller catalyst particles. Furthermore, curve fitting analysis on the EXAFS spectra of NiRu catalysts are performed to estimate whether Ru is atomically mixed with Ni. SI Figure S4 and Table S3 show the curve fitting results and structural parameters of Ni<sub>85</sub>Ru<sub>15</sub> catalyst. The similarity of the coordination number (CN) of Ru–Ru ( $7.3 \pm 2.5$ ) and Ru–Ni ( $8.0 \pm 1.1$ ) in Ni<sub>85</sub>Ru<sub>15</sub> indicates that Ru and Ni are well mixed at the atomic level. The sum of Ru–Ru and Ru–Ni CNs,  $15.3 \pm 3.6$ , revealed that Ru atoms are located in a close packed structure and therefore exist inside the Ni<sub>85</sub>Ru<sub>15</sub> particles. By contrast, the CN of Ni–Ni ( $7.0 \pm 2.1$ ) is significantly larger than that of Ni–Ru ( $1.5 \pm 0.9$ ), and the sum of the two CNs ( $8.5 \pm 3.0$ ) is much less than 12, suggesting that Ni atoms are located on the surface of the particles, which is consistent with the XPS results.

In situ UV–vis spectroscopy was employed to monitor the nucleation and growth process during catalyst preparation. To decrease the absorbance of resulting catalysts solution to a suitable intensity for the equipment, the precursor, PVP, and NaBH<sub>4</sub> solution were diluted to 3/40 of the concentration in typical catalyst preparation conditions. In addition, the temperature was maintained at 16 °C to make the reduction process recordable. In the pure Ni case (Figure 5a), the spectra remain almost the same in the first 10 min, and a sharp increase was observed on the 12 min curve, indicating a very slow nucleation and burst growth process. After that, the shapes of the curves remained identical while the intensity gradually increased in the next 14 min, representing the reduction of remaining Ni<sup>2+</sup>. In contrast, Ru is much easier to reduce (Figure 5b). The curve recorded immediately after the addition of NaBH<sub>4</sub> solution exhibits nanoparticle type absorbance, and the following curves showed slight increments in the intensity. For the Ni<sub>85</sub>Ru<sub>15</sub> catalyst (Figure 5c), the evolution of the spectra resembles that of the pure Ru catalyst. No induction period was observed, indicating that Ru facilitated the reduction of Ni. Plausibly, part of the Ru<sup>3+</sup> was reduced immediately upon addition of

NaBH<sub>4</sub> forming Ru nuclei, which act as catalysts to promote the reduction of Ni<sup>2+</sup> and remaining Ru<sup>3+</sup>, resulting in atomically mixed, ultrasmall NiRu particles. This scenario matches perfectly with XPS and XAS analysis in which Ni was found to be surface-enriched. Chen et al. reported the synthesis of NiRu alloy nanoparticle in oleylamine.<sup>26</sup> A strong reductant, such as LiBEt<sub>3</sub>H, was employed to reduce Ni and Ru precursors simultaneously. Interestingly, our work suggests that Ru exhibits a noble-metal-induced reduction<sup>27</sup> effect, and a mild reducing agent such as NaBH<sub>4</sub> is adequate to produce NiRu bimetallic catalyst without metal segregation.

These instrumentation analyses reveal the following salient structural features of the Ni<sub>85</sub>Ru<sub>15</sub> catalyst: (1) the particle size of the catalyst is significantly smaller than that of monometallic Ni catalyst prepared under identical conditions; (2) Ru atoms stay mostly inside the Ni<sub>85</sub>Ru<sub>15</sub> particles, whereas Ni atoms preferentially stay in the surface; and (3) Ni atoms are electron-enriched, whereas Ru atoms are electron-deficient because of electron donation from Ru to Ni.

A kinetic study of the hydrogenolysis of **1a** over Ni<sub>85</sub>Ru<sub>15</sub> over a period of 2 h was conducted (see Figure 6a and detailed data in

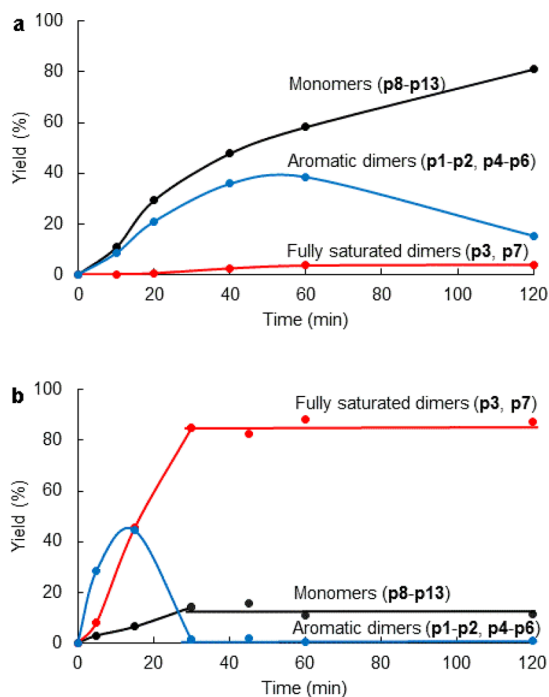


**Figure 6.** Kinetic study on hydrogenolysis of **1a** over (a) Ni<sub>85</sub>Ru<sub>15</sub> and (b) Ru. Reaction conditions: 0.22 mmol of **1a**, 3 mL of freshly prepared aqueous solution containing 0.022 mmol of metal and 0.44 mmol of PVP, 10 bar H<sub>2</sub>, 130 °C.

SI Table S2). Before the substrate was exhausted, no significant drop in activity was observed, indicating Ni<sub>85</sub>Ru<sub>15</sub> was stable. Both monomers and dimers were generated smoothly, revealing first-order kinetics of C–O cleavage as well as hydrogenation. The decrease in the yield of aromatic dimers (containing at least one C<sub>6</sub> aromatic ring) after 60 min implies that these dimers can be further converted into monomers. On the other hand, the yields for fully hydrogenated dimers (**p3**, **p7**) kept increasing, indicating that they cannot be further converted. From the initial linear part of the kinetic curve, the activity of Ni<sub>85</sub>Ru<sub>15</sub> catalyst, defined as the cleaved C–O bond linkage per molar metal (Ni and Ru combined) per hour, was calculated to be 5.8 h<sup>-1</sup>. It is

much higher than the activity of pure Ni (1 h<sup>-1</sup>) catalyst in a previous study under similar conditions.<sup>15e</sup> A kinetic study over pure Ru was also investigated (Figure 6b). Ru showed a comparable initial activity of 3.5 h<sup>-1</sup> in hydrogenolysis of the C–O bond, but the high hydrogenation rate leads to complete saturation of the benzene rings in 30 min. The fully saturated ethers are very hard to break down, hence causing the low yield of monomers. On the basis of the kinetic studies, the entire reaction pathways is illustrated in Scheme 1.

To obtain the intrinsic hydrogenolysis activity of the catalysts (the turnover frequency, TOF), a CS<sub>2</sub> poison titration method was adopted to determine the surface atom fraction. For Ni<sub>85</sub>Ru<sub>15</sub>, hydrogenolysis of 1-benzyloxy-2-methoxybenzene (**2**) was taken as a probe reaction because the representing  $\alpha$ -O-4 type linkage is chemically easier to break down, allowing the reaction to be conducted at lower temperature to benefit the poisoning effect. With increasing amounts of CS<sub>2</sub>, the yield of 2-methoxyphenol dropped gradually (see SI Figure S5). Assuming that each CS<sub>2</sub> molecule blocks two surface atoms, we could determine the surface atom fraction to be 26% for Ni<sub>85</sub>Ru<sub>15</sub>. For the Ru catalyst, the hydrogenation of toluene was chosen to be the probe reaction for the CS<sub>2</sub> poison titration test, and the surface atoms fraction was determined to be 60%. Thus, the TOF in the hydrogenolysis reaction is 5.8 h<sup>-1</sup> and 22 h<sup>-1</sup> for Ru and Ni<sub>85</sub>Ru<sub>15</sub>, respectively, at 130 °C and 10 bar H<sub>2</sub>. Clearly, the TOF of Ni<sub>85</sub>Ru<sub>15</sub> is much higher than pure Ru catalyst and is comparable to the monometallic Ni catalyst (25 h<sup>-1</sup>) under similar reaction conditions. Furthermore, the TOF of the Ni<sub>85</sub>Ru<sub>15</sub> catalyst far exceeds the Ni catalyst under lower temperatures and lower H<sub>2</sub> pressures (vide infra).

Hydrogenolysis reactions at various temperatures over Ni and Ni<sub>85</sub>Ru<sub>15</sub> were conducted. From the Arrhenius plot, the apparent activation energy ( $E_a$ ) for **1a** (Figure 7a) was much lower over the Ni<sub>85</sub>Ru<sub>15</sub> catalyst (46.3 kJ/mol) than over the Ni catalyst (77.3 kJ/mol). The two lines cross at 1000 K/T = 2.514 (e.g., T = 125 °C), which implies that with the incorporation of Ru to Ni, Ni<sub>85</sub>Ru<sub>15</sub> facilitates hydrogenolysis. Although at selected reaction conditions (130 °C), Ni<sub>85</sub>Ru<sub>15</sub> shares a similar TOF with Ni, Ni<sub>85</sub>Ru<sub>15</sub> is more reactive at lower temperatures. For instance, the hydrogenolysis TOF over Ni<sub>85</sub>Ru<sub>15</sub> is 7.2 h<sup>-1</sup> at 100 °C, almost twice that of TOF over pure Ni (3.9 h<sup>-1</sup>). Hydrogenation of toluene over Ru and Ni<sub>85</sub>Ru<sub>15</sub> were also investigated. The experiments were carried out at high stirring speed to rule out mass transfer limitations (see SI Figure S8 for the effect of stirring speed). As shown in Figure 7b, the  $E_a$  over Ru is very low (5.7 kJ/mol), but it went up to 24.1 kJ/mol over Ni<sub>85</sub>Ru<sub>15</sub>. Nandanwar<sup>28</sup> et al. obtained an  $E_a$  of 27.9 kJ/mol for benzene hydrogenation employing Ru/ $\gamma$ -Al<sub>2</sub>O<sub>3</sub>. In another report,<sup>29</sup> the  $E_a$  for benzene hydrogenation over RuNi/C is 42.1 kJ/mol. Although our data do not match exactly with the literature, the trend is the same. Incorporation of Ni into Ru significantly increases the activation energy for benzene ring hydrogenation. Taken together, the combination of Ni and Ru promotes hydrogenolysis of Ni and inhibits hydrogenation of Ru.

Next, the effect of H<sub>2</sub> pressure was investigated. The product distribution for hydrogenolysis of **1a** was recorded at 30 min reaction time over Ni<sub>85</sub>Ru<sub>15</sub> at 130 °C with varying H<sub>2</sub> pressures. With lower H<sub>2</sub> pressure, higher monomer yields were achieved (see Figure 8). The reaction could even take place with 1 bar H<sub>2</sub>, which is significantly different from the catalytic performance over pure Ni catalyst and Ni/SiO<sub>2</sub>,<sup>15e</sup> which were inactive at ambient pressure. Apparently, Ni<sub>85</sub>Ru<sub>15</sub> enables facile H<sub>2</sub> absorption, and the rate-determining step becomes H<sub>2</sub>

## Scheme 1. Proposed Reaction Pathways of 1a Hydrogenolysis/Hydrogenation into Monomeric and Dimeric Products

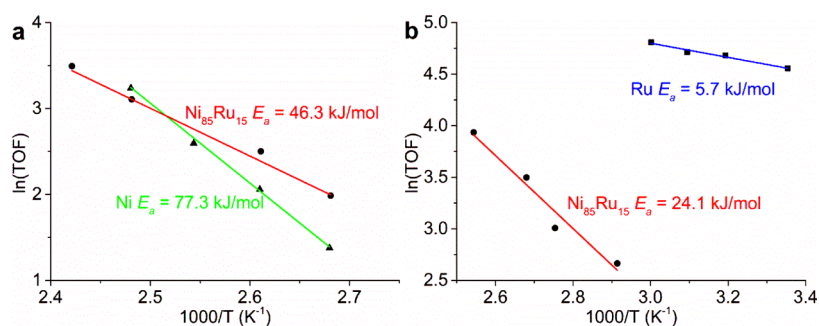
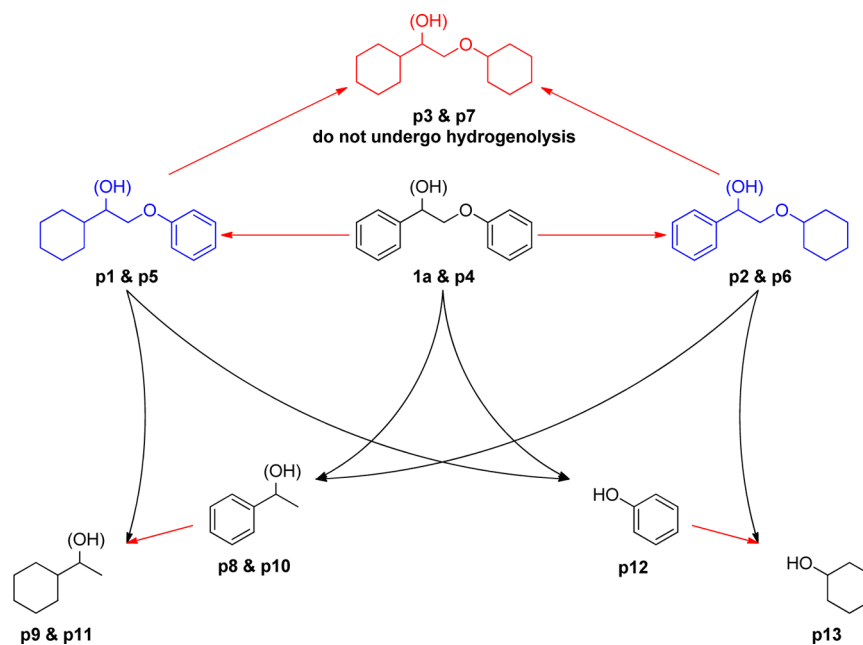


**Figure 7.** (a) Arrhenius plots for hydrogenolysis of **1a** over Ni and Ni<sub>85</sub>Ru<sub>15</sub>. Reaction conditions: 0.22 mmol of **1a**, 3 mL of freshly prepared aqueous solution containing 0.022 mmol of metal and 0.44 mmol of PVP, 10 bar H<sub>2</sub>, 30 min. (b) Arrhenius plots for hydrogenation of toluene over Ru and Ni<sub>85</sub>Ru<sub>15</sub>. Reaction conditions: 2.2 mmol of toluene, 3 mL of freshly prepared aqueous solution containing 0.022 mmol of metal and 0.44 mmol of PVP, 10 bar H<sub>2</sub>, 30 min.

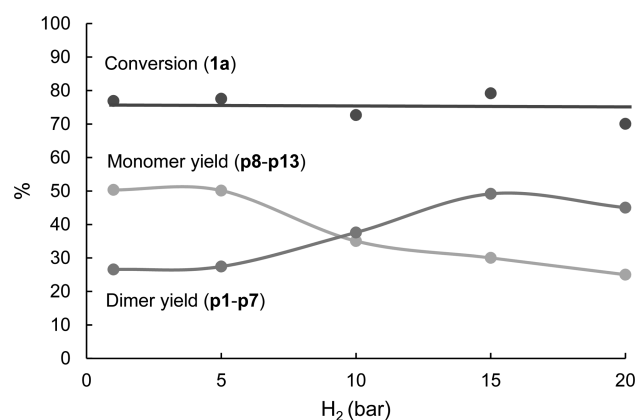


**Figure 8.** Conversions and products distributions over Ni<sub>85</sub>Ru<sub>15</sub> as functions of H<sub>2</sub> pressure. Reaction conditions: 0.22 mmol of **1a**, 3 mL of freshly prepared aqueous solution containing 0.022 mmol of metal and 0.44 mmol of PVP, 130 °C, 30 min.

pressure-independent. The yield of the monomers dropped with more than 5 bar H<sub>2</sub> pressure, indicating that hydrogenation and hydrogenolysis reactions are competing with the same active

sites on Ni<sub>85</sub>Ru<sub>15</sub> catalyst, and higher H<sub>2</sub> pressure prefers hydrogenation.<sup>15e</sup> When H<sub>2</sub> pressure is >15 bar, monomer and dimer yields were both decreased due to the high coverage of hydrogen on catalyst surface inhibiting the adsorption of substrates.

Other model compounds were also tested over Ni<sub>85</sub>Ru<sub>15</sub>. As shown in SI Figure S6, **1b** with one methoxy group on B ring had a conversion of 90% after 1 h under typical reaction conditions, with a total monomer yield of 55%. The slightly lower reactivity could be attributed to the steric hindrance of the methoxy group. Interestingly, **1c** with two methoxy groups on the B ring was converted completely with a higher total monomer yield (72%). For the weakest linkage type in lignin,  $\alpha$ -O-4, the represented substrate **2** is hydrogenolyzed, even at 60 °C over Ni<sub>85</sub>Ru<sub>15</sub>. In addition, without using harsher reaction conditions, substrate **3**, representing the strongest C–O linkage, 4-O-5, was converted at 130 °C, yielding 10% monomers (SI Figure S6).

**NiRh and NiPd Catalysts.** Following a similar preparation procedure, NiRh catalysts with various Rh contents were synthesized and evaluated in hydrogenolysis of **1a**. As shown in Figure 9a, the Rh monometallic catalyst exhibited high activity (100% conversion) and low selectivity (22%) toward monomers.

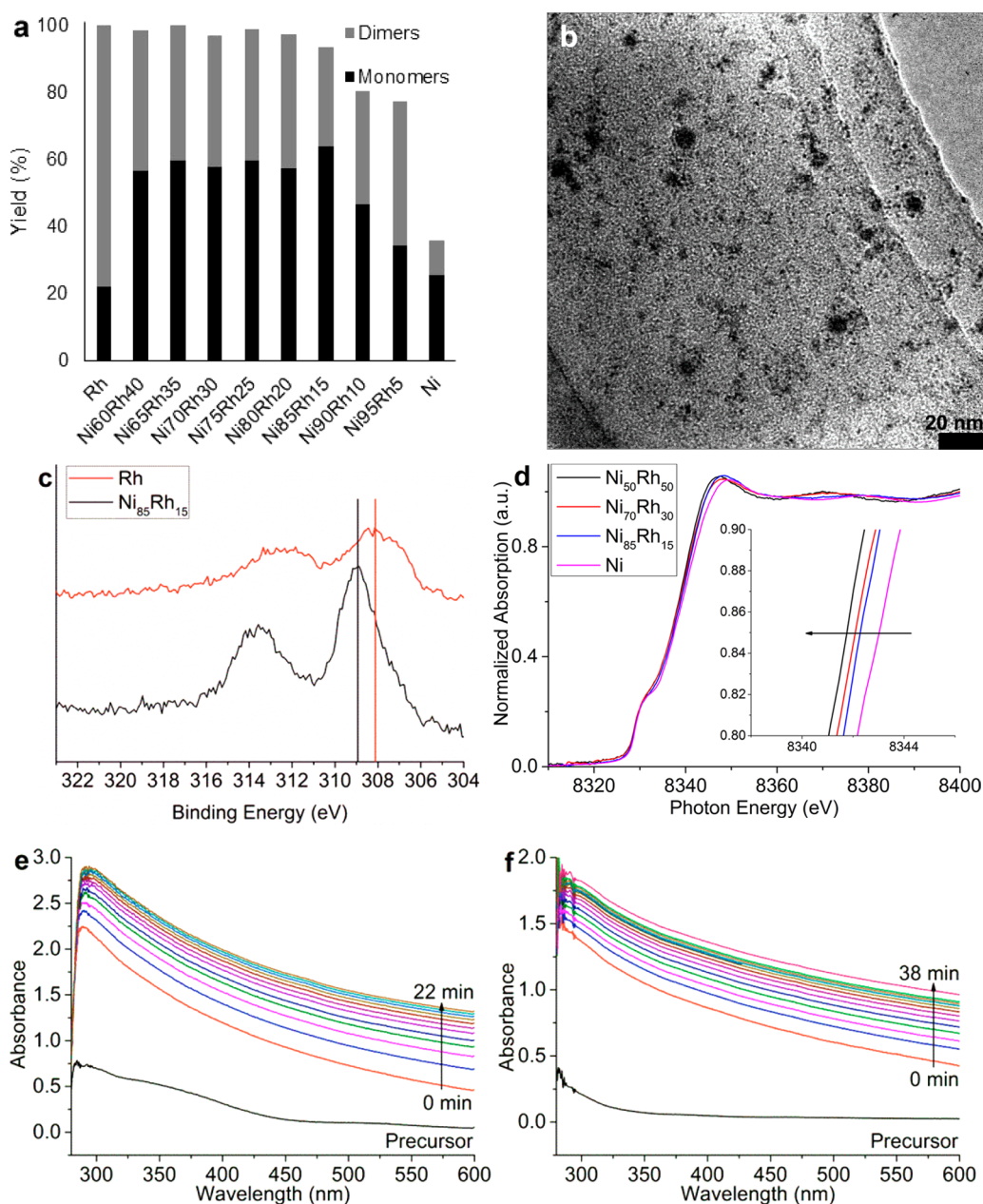


**Figure 9.** (a) Yields of monomers and dimers over Ni, Rh, and NiRh with varying Ni/Rh ratios. Reaction conditions: 0.22 mmol of **1a**, 3 mL of freshly prepared aqueous solution containing 0.022 mmol of metal and 0.44 mmol of PVP, 10 bar  $H_2$ , 130 °C, 1 h. (b) TEM image of  $Ni_{85}Rh_{15}$ . (c) XPS spectra for Rh (red curve) and  $Ni_{85}Rh_{15}$  (black curve) at Rh 3d region. (d) Ni K-edge XANES spectra of Ni,  $Ni_{85}Rh_{15}$ ,  $Ni_{70}Rh_{30}$ ,  $Ni_{50}Rh_{50}$  catalysts. In situ UV-vis spectra recorded during the preparation of (e) Rh and (f)  $Ni_{85}Rh_{15}$  catalysts. Spectra were recorded every 2 min. Reaction conditions: 2 mL of water solution containing 0.00165 mmol of metal precursors and 0.033 mmol of PVP and 1 mL of  $NaBH_4$  (0.00825 mmol) solution were added; pure water as reference.

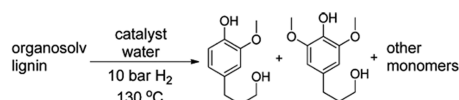
The synergistic effect was again observed in NiRh bimetallic catalysts. The activity increased with increasing Rh content and reached its highest point with  $Ni_{85}Rh_{15}$ , over which 94% conversion with 64% monomer yield was achieved. To further verify the synergistic effect,  $Ni_{85}Pd_{15}$  was prepared and evaluated in hydrogenolysis of **1a**, achieving complete conversion and 95.7% monomer yield. Note that the conversion was 100% but the monomer yield was only 12.1% over pure Pd catalyst.

A variety of instrumentation analyses were carried out to reveal the structural features of the NiRh catalysts. TEM analysis indicates that a majority of the  $Ni_{85}Rh_{15}$  catalyst had particle sizes of  $\sim 2$  nm, and some had sizes of  $\sim 10$  nm (Figure 9b). In the XPS spectra (Figure 9c), the  $3d_{5/2}$  binding energy of Rh shifted from

308.2 eV in the Rh catalysts to 308.9 eV in  $Ni_{85}Rh_{15}$ , indicating electron transfer from Rh to Ni. This was further corroborated by XANES analysis, that is, the Ni K-edge shifts toward a lower energy as the Rh content increases (see Figure 9d). The in situ UV-vis (Figure 9e,f) suggests Rh accelerated Ni reduction. Combined, it appears that the role that Rh played in  $Ni_{85}Rh_{15}$  was similar to that of Ru in the  $Ni_{85}Ru_{15}$  catalyst.

**Hydrogenolysis of Real Lignin over Ni, M and NiM Catalysts.** Encouraged by the results of model compound hydrogenolysis, we next conducted reactions on organosolv lignin from *Betula platyphylla* suk. As shown in Table 1, under the typical reaction conditions, 0.8 wt % monomeric products yield was achieved at 1 h over  $Ni_{85}Ru_{15}$ . In contrast, 0.16 wt %



Table 1. Organosolv Lignin Depolymerization over Ni, Ru, Rh, Pd, Ni<sub>85</sub>Ru<sub>15</sub>, Ni<sub>85</sub>Rh<sub>15</sub>, and Ni<sub>85</sub>Pd<sub>15</sub> Catalysts in Water<sup>a</sup>


catalyst	time (h)	yield (wt %)			residual lignin (wt %)
Ni	1	0	0	0	46
Ru	1	0.1	0.03	0.03	50
Ni <sub>85</sub> Ru <sub>15</sub>	1	0.1	0.6	0.1	58
Ni <sub>85</sub> Ru <sub>15</sub>	12	1.4	5.0	0.4	56
Ru	12	0.2	0.06	0.6	38
Rh	1	0.1	0.1	0.07	52
Pd	1	0.06	0.3	0.1	57
Ni <sub>85</sub> Rh <sub>15</sub>	1	0.5	2.0	0.1	50
Ni <sub>85</sub> Rh <sub>15</sub>	12	0.7	2.2	0.7	51
Ni <sub>85</sub> Pd <sub>15</sub>	1	0.2	1.6	0.6	52
Ni <sub>85</sub> Pd <sub>15</sub>	12	0.9	3.3	0.4	44

<sup>a</sup>Reaction conditions: 50 mg of organosolv lignin, 3 mL of freshly prepared aqueous solution containing 0.022 mmol metal and 0.44 mmol PVP, 10 bar H<sub>2</sub>. Reaction temperature and time can be found in the table.

monomers was obtained over pure Ru catalyst, and no monomeric products could be identified after the reaction over pure Ni under the same reaction conditions. By prolonging the reaction time to 12 h, a monomeric product yield of 6.8 wt % could be obtained over Ni<sub>85</sub>Ru<sub>15</sub>. In contrast, the monomeric yield over Ru reached only 0.2 wt % at 1 h and 0.9 wt % at 12 h. Over Ni<sub>85</sub>Rh<sub>15</sub> and Ni<sub>85</sub>Pd<sub>15</sub>, 2.6 and 2.4 wt % monomeric product yields were achieved after 1 h, in sharp contrast to the monomeric product yields of 0.27 and 0.46 wt % over pure Rh and Pd catalysts, respectively. Recently, Song et al.<sup>8b</sup> reported that lignin from intact birch biomass could be converted to monomeric phenols with ~50% yield at 200 °C using Ni/C catalysts in hydrogen-donating alcohols. Toledano et al.<sup>15h,30</sup> conducted microwave-assisted lignin hydrogenolysis, achieving an impressive 17% monomeric chemical yield at 140 °C over Ni/AlSBA catalyst in tetralin. Kou et al.<sup>31</sup> reported the depolymerization of organosolv lignin under harsher reaction conditions with Rh/C achieving 5.6 wt % monomeric product yields. The performance of catalytic systems with varying lignin from different sources and pretreatments are incomparable. Nevertheless, low reaction temperature (130 °C) and pure water as the solvent are the salient advantages of this study. A very recent paper suggests that organosolve lignin contains a fraction of monomers itself;<sup>32</sup> however, we are confident that the aromatic monomers observed in our catalytic system were not originally present in the organosolve lignin, on the basis of the following facts: (1) no monomers were detected in the absence of catalysts;<sup>16</sup> (2) different catalysts provided significantly different monomer yields (see Table 1); and (3) GPC analysis indicated that the organosolv lignin we used for the reaction is of polymeric nature (see SI Figure S9).

Because GC is able to detect only small-molecule compounds, selected crude products were further characterized by FTIR (See SI Figure S7). The intensity of the C–O bond vibration in the guaiacyl unit<sup>33</sup> at 1272 cm<sup>-1</sup>, which is indicative of the integrity of the lignin structure, remained unaltered after reaction over the Ni catalyst but decreased after reaction over Ni<sub>85</sub>Ru<sub>15</sub>, further confirming that Ni<sub>85</sub>Ru<sub>15</sub> is more active in breaking the C–O bond. Over the Ru catalyst, the relative intensity of the IR peaks from 1607 to 1423 cm<sup>-1</sup>, attributed to vibration of the aromatic ring skeleton,<sup>34</sup> decreased after reaction, implying benzene ring hydrogenation. The intensity of peak at 1272 cm<sup>-1</sup> also

decreased, which is not unreasonable because the guaiacyl unit does not exist after benzene ring hydrogenation. Another significant change in the spectra is the disappearance or decrease in the peak at 1710 cm<sup>-1</sup>, which was assigned to nonconjugated C=O vibration,<sup>35</sup> indicating hydrogenation of the C=O bond over all three catalysts. Overall, the performances of Ni, M, and Ni<sub>85</sub>M<sub>15</sub> catalysts over lignin model compounds and real lignin are consistent, that is, Ni<sub>85</sub>M<sub>15</sub> is more active and selective compared with single-component catalysts.

## CONCLUSIONS

A series of bimetallic Ni<sub>85</sub>M<sub>15</sub> (M = Ru, Rh, and Pd) catalysts were demonstrated to be effective in the hydrogenolysis of lignin model compounds and organosolv lignin under mild reaction conditions in water. Single-component Ni and the noble metal catalysts are active for this reaction, but the combination of the two exhibits prominent effects overcoming the limitations of a single component catalyst. Among the three, Ni<sub>85</sub>Ru<sub>15</sub> was fully investigated, and the synergistic effects include

- (1) Incorporation of 15% Ru induces a dramatically enhanced reduction rate of Ni in the catalyst synthesis, resulting in atomically mixed, ultrasmall bimetallic catalyst particles with considerably increased surface atom fractions, which accordingly leads to high catalytic activity.
- (2) Fully hydrogenated dimeric compounds do not undergo further C–O hydrogenolysis under applied conditions, and the high hydrogenation activity is one of the main limitations for noble metal catalysts. However, the undesired hydrogenation of the aromatic ring is greatly inhibited over the Ni<sub>85</sub>Ru<sub>15</sub> catalyst compared with the pure Ru catalyst, leading to a high yield of aromatic monomeric compounds.
- (3) Ni<sub>85</sub>Ru<sub>15</sub> catalyst exhibits a much higher TOF at low temperatures (for example, 100 °C) or low H<sub>2</sub> pressure (1 bar) compared with the pure Ni catalyst. This exceptionally low-temperature, low-pressure activity in lignin hydrogenolysis plausibly arises from enhanced activation of H<sub>2</sub> and substrate due to electron-enriched Ni.

## ■ ASSOCIATED CONTENT

## ■ Supporting Information

Detailed reaction data, TEM, XRD, XPS, EXAFS fitting results and FTIR are provided as Supporting Information. This material is available free of charge via the Internet at <http://pubs.acs.org>.

## ■ AUTHOR INFORMATION

## Corresponding Author

\*E-mail: [ning.yan@nus.edu.sg](mailto:ning.yan@nus.edu.sg).

## Notes

The authors declare no competing financial interest.

## ■ ACKNOWLEDGMENTS

This work is financially supported by the A\*Star PSF project (WBS: R-279-000-403-305) and a MOE Tier-1 project (WBS: R-279-000-387-112). XAS experiments were performed at the beamline NW10A, Photon Factory Advanced Ring (PF-AR), KEK, Tsukuba, Japan, under the approval of the Photon Factory Advisory Committee (Proposal No. 2012G601) and at the beamline BL01B1, Spring-8, Hyogo, Japan under the approval of Japan Synchrotron Radiation Research Institute (JASRI) (Proposal No. 2013B1405).

## ■ REFERENCES

- (1) Sanderson, K. *Nature* **2011**, *474*, S12–S14.
- (2) Sarkanen, K. V.; Ludwig, C. H. *Lignins: Occurrence, Formation, Structure and Reactions*; Wiley-Interscience: New York, 1971.
- (3) (a) Rahimi, A.; Azarpira, A.; Kim, H.; Ralph, J.; Stahl, S. S. *J. Am. Chem. Soc.* **2013**, *135*, 6415–6418. (b) Gao, Y.; Zhang, J.; Chen, X.; Ma, D.; Yan, N. *ChemPlusChem*. **2014**, DOI: 10.1002/cplu.201300439. (c) Jia, S.; Cox, B. J.; Guo, X.; Zhang, Z. C.; Ekerdt, J. G. *ChemSusChem* **2010**, *3*, 1078–1084. (d) Dee, S.; Bell, A. T. *Green Chem.* **2011**, *13*, 1467–1475.
- (4) (a) Corma, A.; Iborra, S.; Velty, A. *Chem. Rev.* **2007**, *107*, 2411–2502. (b) Ruppert, A. M.; Weinberg, K.; Palkovits, R. *Angew. Chem., Int. Ed.* **2012**, *51*, 2564–2601. (c) Kobayashi, H.; Komanoya, T.; Guha, S. K.; Hara, K.; Fukuoka, A. *Appl. Catal., A* **2011**, *409–410*, 13–20. (d) Yan, N.; Dyson, P. J. *Curr. Opin. Chem. Eng.* **2013**, *2*, 178–183.
- (5) Holladay, J. E.; White, J. F.; Bozell, J. J.; Johnson, D. *Top Value-Added Chemicals from Biomass; Vol. II, Results of Screening for Potential Candidates from Biorefinery Lignin*; Northwest National Laboratory: Richland, WA, 2007.
- (6) Besson, M.; Gallezot, P.; Pinel, C. *Chem. Rev.* **2014**, *114*, 1827–1870.
- (7) (a) Parsell, T. H.; Owen, B. C.; Klein, I.; Jarrell, T. M.; Marcum, C. L.; Hauptert, L. J.; Amundson, L. M.; Kenttamaa, H. I.; Ribeiro, F.; Miller, J. T.; Abu-Omar, M. M. *Chem. Sci.* **2013**, *4*, 806–813. (b) Chatterjee, M.; Ishizaka, T.; Suzuki, A.; Kawanami, H. *Chem. Commun.* **2013**, *49*, 4567–4569. (c) Xu, W.; Miller, S. J.; Agrawal, P. K.; Jones, C. W. *ChemSusChem* **2012**, *5*, 667–675. (d) Wu, A.; Patrick, B. O.; Chung, E.; James, B. R. *Dalton Trans.* **2012**, *41*, 11093–11106.
- (8) (a) Strassberger, Z.; Alberts, A. H.; Louwse, M. J.; Tanase, S.; Rothenberg, G. *Green Chem.* **2013**, *15*, 768. (b) Song, Q.; Wang, F.; Cai, J.; Wang, Y.; Zhang, J.; Yu, W.; Xu, J. *Energy Environ. Sci.* **2013**, *6*, 994–1007. (c) Cornella, J.; Gómez-Bengoa, E.; Martin, R. *J. Am. Chem. Soc.* **2013**, *135*, 1997–2009. (d) Wang, X.; Rinaldi, R. *ChemSusChem* **2012**, *5*, 1455–1466. (e) Sergeev, A. G.; Webb, J. D.; Hartwig, J. F. *J. Am. Chem. Soc.* **2012**, *134*, 20226–20229. (f) Li, C.; Zheng, M.; Wang, A.; Zhang, T. *Energy Environ. Sci.* **2012**, *5*, 6383–6390. (g) Gosselink, R. J. A.; Teunissen, W.; van Dam, J. E. G.; de Jong, E.; Gellerstedt, G.; Scott, E. L.; Sanders, J. P. M. *Bioresour. Technol.* **2012**, *106*, 173–177. (h) Tobisu, M.; Chatani, N. *ChemCatChem*. **2011**, *3*, 1410–1411. (i) Kleinert, M.; Barth, T. *Chem. Eng. Technol.* **2008**, *31*, 736–745. (j) Feng, B.; Kobayashi, H.; Ohta, H.; Fukuoka, A. *J. Mol. Catal. A: Chem.* **2014**, DOI: 10.1016/j.molcata.2013.09.025.
- (9) Yan, N.; Zhao, C.; Dyson, P. J.; Wang, C.; Liu, L.-t.; Kou, Y. *ChemSusChem* **2008**, *1*, 626–629.
- (10) Ye, Y.; Zhang, Y.; Fan, J.; Chang, J. *Bioresour. Technol.* **2012**, *118*, 648–651.
- (11) Zhao, C.; Lercher, J. A. *ChemCatChem*. **2012**, *4*, 64–68.
- (12) (a) Guerrero, M.; Coppel, Y.; Chau, N. T. T.; Roucoux, A.; Denicourt-Nowicki, A.; Monflier, E.; Bricout, H.; Lecante, P.; Philippot, K. *ChemCatChem*. **2013**, *5*, 3802–3811. (b) Yuan, Y.; Yan, N.; Dyson, P. J. *ACS Catal.* **2012**, *2*, 1057–1069. (c) González-Gálvez, D.; Nolis, P.; Philippot, K.; Chaudret, B.; van Leeuwen, P. W. N. M. *ACS Catal.* **2012**, *2*, 317–321.
- (13) Barta, K.; Warner, G. R.; Beach, E. S.; Anastas, P. T. *Green Chem.* **2014**, *15*, 191–196.
- (14) Rensel, D. J.; Rouvimov, S.; Gin, M. E.; Hicks, J. C. *J. Catal.* **2013**, *305*, 256–263.
- (15) (a) Sergeev, A. G.; Hartwig, J. F. *Science* **2011**, *332*, 439–443. (b) Roberts, V. M.; Knapp, R. T.; Li, X.; Lercher, J. A. *ChemCatChem*. **2010**, *2*, 1407–1410. (c) Roberts, V. M.; Stein, V.; Reiner, T.; Lemonidou, A.; Li, X.; Lercher, J. A. *Chem.—Eur. J.* **2011**, *17*, 5939–5948. (d) Roberts, V.; Fendt, S.; Lemonidou, A. A.; Li, X.; Lercher, J. A. *Appl. Catal., B* **2010**, *95*, 71–77. (e) He, J.; Zhao, C.; Lercher, J. A. *J. Am. Chem. Soc.* **2012**, *134*, 20768–20775. (f) Song, Q.; Wang, F.; Xu, J. *Chem. Commun.* **2012**, *48*, 7019–7021. (g) Sturgeon, M. R.; O'Brien, M. H.; Ciesielski, P. N.; Katahira, R.; Kruger, J. S.; Chmely, S. C.; Hamlin, J.; Lawrence, K.; Hunsinger, G. B.; Foust, T. D.; Baldwin, R. M.; Bidy, M. J.; Beckham, G. T. *Green Chem.* **2014**, *16*, 824–835. (h) Toledano, A.; Serrano, L.; Pineda, A.; Romero, A. A.; Luque, R.; Labidi, J. *Appl. Catal., B* **2014**, *145*, 43–55.
- (16) Zhang, J.; Asakura, H.; van Rijn, J.; Yang, J.; Duchesne, P.; Zhang, B.; Chen, X.; Zhang, P.; Saeys, M.; Yan, N. *Green Chem.* **2014**, DOI: 10.1039/C3GC42589D.
- (17) (a) Sinfelt, J. H. *J. Catal.* **1973**, *29*, 308–315. (b) Sinfelt, J. H. *Acc. Chem. Res.* **1977**, *10*, 15–20.
- (18) Ravel, B.; Newville, M. *J. Synchrotron Radiat.* **2005**, *12*, 537–541.
- (19) Zabinsky, S. I.; Rehr, J. J.; Ankudinov, A.; Albers, R. C.; Eller, M. J. *Phys. Rev. B* **1995**, *52*, 2995–3009.
- (20) (a) Zhang, J.; Yuan, Y.; Kilpin, K. J.; Kou, Y.; Dyson, P. J.; Yan, N. *J. Mol. Catal. A: Chem.* **2013**, *371*, 29–35. (b) Yan, N.; Yuan, Y.; Dyson, P. J. *Chem. Commun.* **2011**, *47*, 2529–2531.
- (21) Nichols, J. M.; Bishop, L. M.; Bergman, R. G.; Ellman, J. A. *J. Am. Chem. Soc.* **2010**, *132*, 12554–12555.
- (22) Scanlon, J. T.; Willis, D. E. *J. Chromatogr. Sci.* **1985**, *23*, 333–340.
- (23) Pepper, J. M.; Siddiqueullah, M. *Can. J. Chem.* **1961**, *39*, 1454–1461.
- (24) Yuan, Y.; Yan, N.; Dyson, P. J. *Inorg. Chem.* **2011**, *50*, 11069–11074.
- (25) Frenkel, A. I. *Chem. Soc. Rev.* **2012**, *41*, 8163–8178.
- (26) Chen, G.; Desinan, S.; Rosei, R.; Rosei, F.; Ma, D. *Chem.—Eur. J.* **2012**, *18*, 7925–7930.
- (27) Wang, D.; Li, Y. *J. Am. Chem. Soc.* **2010**, *132*, 6280–6281.
- (28) Nandanwar, S. U.; Chakraborty, M.; Mukhopadhyay, S.; Shenoy, K. T. *React. Kinet. Mech. Catal.* **2013**, *108*, 473–489.
- (29) Zhu, L.; Zheng, L.; Du, K.; Fu, H.; Li, Y.; You, G.; Chen, B. H. *RSC Adv.* **2013**, *3*, 713–719.
- (30) Toledano, A.; Serrano, L.; Balu, A. M.; Luque, R.; Pineda, A.; Labidi, J. *ChemSusChem* **2013**, *6*, 529–536.
- (31) Liu, L.-T.; Zhang, B.; Li, J.; Ma, D.; Kou, Y. *Acta Phys. Chim. Sin.* **2012**, *28*, 2343–2348.
- (32) Jarrell, T. M.; Marcum, C. L.; Sheng, H.; Owen, B. C.; O'Lenick, C. J.; Maraun, H.; Bozell, J. J.; Kenttamaa, H. I. *Green Chem.* **2014**, DOI: 10.1039/C3GC42355G.
- (33) Jung, H. J. G.; Himmelsbach, D. S. *J. Agric. Food. Chem.* **1989**, *37*, 81–87.
- (34) Zhang, A.-P.; Liu, C.-F.; Sun, R.-C. *Ind. Crops Prod.* **2010**, *31*, 357–362.
- (35) Derkacheva, O.; Sukhov, D. *Macromol. Symp.* **2008**, *265*, 61–68.